Supplemental Materials

Hyun-Myung Chun[1], Sungmin Hwang[2], Byungnam Kahng[3], Heiko Rieger[4,5], and Jae Dong Noh[6]

[1] *School of Physics, Korea Institute for Advanced Study, Seoul 02455, Korea*
[2] *Capital Fund Management, 75007 Paris, France*
[3] *Center for Complex Systems Studies, and KENTECH Institute for Grid Modernization, Korea Institute of Energy Technology, Naju 58217, Korea*
[4] *Center for Biophysics and Department of Theoretical Physics, Saarland University, 66123 Saarbrücken, Germany*
[5] *Lebniz-Institute for New Materials INM, 66123 Saarbrücken, Germany*
[6] *Department of Physics, University of Seoul, Seoul 02504, Korea*

Appendix A: Distribution of the Random Walk Centrality

We investigate statistical properties of the random walk centrality or the accessibility index of sites in the 2D critical percolation cluster. Given a percolation cluster, we measure the accessibility indices α of all sites and construct a histogram of them normalized by the average value $\langle\alpha\rangle$. The probability distribution function $P(\alpha/\langle\alpha\rangle)$ is then obtained by taking the average of the histogram over the ensemble of percolation clusters. In Fig. S1(a), we present and compare the distribution functions at three different values of L. They overlap one another, which indicates that the accessibility distribution is characterized with only a single scale, namely the mean value $\langle\alpha\rangle$. The distribution function has asymmetric Gaussian tails.

We also study the system size dependence of the mean value $\langle\alpha\rangle$, the minimum value α_H of the hub, and the maximum value α_M of the marginal site. Their ensemble averaged values follow the power law $\alpha \sim L^{2.88(1)}$ with the same exponent close to the random walk exponent d_w. The accessibility index α_i has a meaning of the average MFPT to i from all the other sites. It is surprising that the average MFPT to the most accessible site (hub) and the least accessible site (marginal site) follow the finite-size scaling law with the same exponent. This indicates that the average quantity alone is not a useful measure. The structural heterogeneity is not captured by the finite size scaling behavior of the average MFPT.

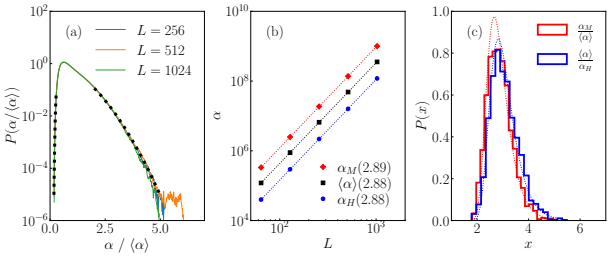

FIG. S1. (a) Distribution functions of the normalized accessibility index. The tails are fitted well by Gaussian functions (dashed lines) with different stiffness on either side. (b) System size dependence of the accessibility indices of the hub (α_H), the marginal site (α_M), and the mean value ($\langle\alpha\rangle$). The figure in the legend refers to the finite-size scaling exponent. (c) Distribution functions (solid lines) of the largest accessibility index and the largest random walk centrality (inverse accessibility index). They are compared with the Gumbel distribution function (dotted lines) $P_G(x) = \exp\left[(x-\mu)/\beta - e^{-(x-\mu)/\beta}\right]/\beta$ with μ and β being determined from the mean and the variance of the data.

Figure S1(c) presents the distribution functions of the maximum accessibility index $\alpha_M/\langle\alpha\rangle$ and the maximum random walk centrality $\langle\alpha\rangle/\alpha_H$, normalized with $\langle\alpha\rangle$. The distribution functions are comparable with the Gumbel distribution which governs the extreme value statistics of Gaussian-distributed random variables.

Appendix B: Distance Dependent MFPT

We have shown in the main text the MFPTs from the hub and the marginal site follow a power law scaling

$$T(r) \sim L^{\Delta} r^{\theta} \tag{S1}$$

with distinct scaling exponents $(\Delta_h, \theta_h) \simeq (1.90, 0.97)$ for the hub and $(\Delta_m, \theta_m) \simeq (2.36, 0.49)$ for the marginal site. We also measure $T_A(r)$, the average MFPT from an arbitrary source site selected *at random* (see App. C). As shown in Fig. S2(a), $T_A(r)$ also follows the scaling law of Eq. (S1). The scaling exponent is obtained from an effective exponent analysis. The MFPTs within the range $r/\sqrt{2} < r_0 < \sqrt{2}r$ are fitted to yield the effective exponent $\theta(r)$. Figure S2(c) presents the effective exponents for θ_h for the hub, θ_h for the marginal site, and θ_r for a random site. The asymptotic scaling exponent is given by the limiting value in the $r \to \infty$ and $L \to \infty$ limit. The effective exponents for θ_h and θ_m converge to the values obtained from the global fitting in the main text. The effective exponent for θ_r converges to $\theta_r \simeq 0.88$. The three distinct scaling exponents θ_h, θ_m, and θ_r signify the strong structural heterogeneity in the first passage processes.

The strong heterogeneity weakens when one adopts the chemical distance instead of the Euclidean distance as seen in Fig. S2(b) and (d). The chemical distance dependent scaling behavior will be discussed in App. E.

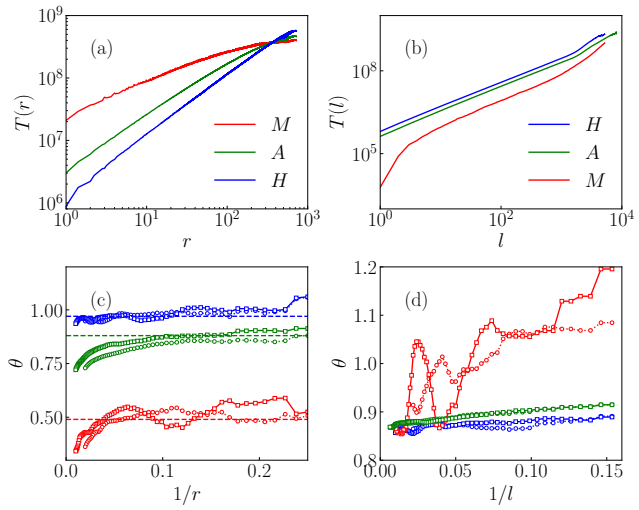

FIG. S2. (a) Euclidean distance (r) dependence and (b) chemical distance (l) dependence of the MFPTs from the hub (H), the marginal site (M), and an arbitrary site selected at random (A) at $L = 1024$. (c) The effective exponents for the power law scaling $T(r) \sim r^{\theta}$ at $L = 512$ (circular symbols) and $L = 1024$ (square symbols). The asymptotic values are marked with the dashed lines. (d) The effective exponents for the power law scaling $T(l) \sim l^{\theta_l}$ at $L = 512$ (circular symbols) and $L = 1024$ (square symbols).

Appendix C: MFPT from a random site

We study the outbound MFPT from a set of sites $\{A_1, A_2, \cdots\}$ where A_n is an arbitrary site selected randomly among the sites at a distance $R_n = 2^{n-1}$ from the hub for 2D critical percolation clusters. We found that the MFPT $T'_n(r)$ from A_n also exhibits the crossover scaling of the form (6) of the main text. In Fig. S3(a), we plot the ratio of $T'_n(r)$ to $T_h(r)$, MFPT from the hub, to highlight the crossover. It clearly shows that $T'_n(r)/T_h(r)$ deviates from 1 for $r \ll R_n$ and converges to 1 for $r \gg R_n$. Interestingly, the scaling exponent in the regime $r \ll R_n$ is given by $\theta_a \simeq 0.84(5) \neq \theta_m$. It is close to θ_h, but not the same.

We also study outbound MFPT from a source site A selected at *completely random* among all sites. In Fig. S3(b), we compare the mean value $T_A(r)$ and the standard deviation $\delta T_A(r)$ of the MFPTs from A to sites at a distance r. $T_A(r)$ corresponds to the MFPT averaged over all source-target pairs. It obeys a power law scaling $T_A(r) \sim r^{\theta_r}$ with a single exponent $\theta_r \simeq 0.88$, which is close to $d_w - d_f$. However, the standard deviation is even larger than the mean value for $r \ll L$. This strong non-self-averaging behavior is another indication of the heterogeneity.

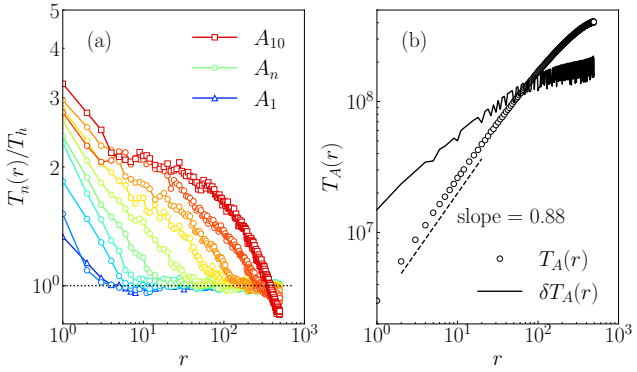

FIG. S3. (a) MFPT $T'_n(r)$ from an arbitrary site A_n at a distance $R_n = 2^{n-1}$ from the hub normalized by $T_h(r)$. The horizon dotted line is a guide to the eye. (b) MFPT $T_A(r)$ from an arbitrary source site selected randomly. If follows a power law scaling $T_A(r) \sim r^{\theta_r}$ with $\theta_r \simeq 0.88$.

Appendix D: Direct and indirect explorations

We demonstrate a qualitative change in the ensemble of first-passage trajectories as the source-target distance increases. We focus on the 2D critical percolation clusters in L^2 square lattices. On a percolation cluster, we first determine the source site s whose RWC is lowest among those at a distance $r_{h-s} = L/8$ from the hub, the maximum RWC site. We then choose randomly a target site t among those at a distance r_{s-t} from s. We generate $1024 \times L$ random walk trajectories starting at s, and compute the fraction f_{viaH} of trajectories visiting the hub before arriving at t.

Figure S4 (a) shows the fraction $\langle f_{\text{viaH}} \rangle$ averaged over 1000 percolation clusters. The average fraction seems to converge to a finite value in the large L limit and increases gradually as r_{s-t} increases. The probability of following indirect paths via the hub increases as r_{s-t} increases.

The distribution function shown in Fig. S4 (b) signifies a qualitative change. It is characterized by two peaks at $f_{\text{viaH}} = 0$ and 1, which reflect the dominance of direct and indirect paths via the hub, respectively. In the short distance regime ($r_{s-t} \lesssim r_{s-h}$), both peaks are evident. The double peak structure indicates strong sample-to-sample fluctuations in the ensemble of percolation clusters and the locations of source-target pairs. As r_{s-t}/r_{s-h} increases, the peak at $f_{\text{viaH}} = 0$ diminishes, leaving only a single peak at $f_{\text{viaH}} = 1$ in the long-distance regime ($r_{s-t} \gtrsim r_{s-h}$). The distribution function is clear evidence for the crossover from the direct exploration in the short distance regime to the indirect exploration via the hub in the long distance regime at the trajectory level.

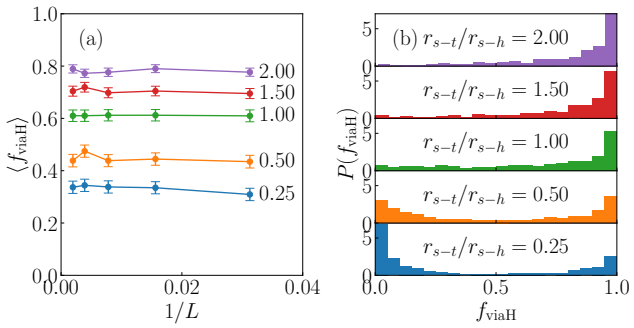

FIG. S4. (a) Average fraction $\langle f_{\rm viaH}\rangle$ of random walk trajectories starting from the local minimum RWC site s and arriving at the target site t via the hub. The distance between the hub and s is $r_{s-h} = L/8$, and the relative distances between s and t are $r_{s-t}/r_{s-h} = 0.25, \cdots, 2.00$. (b) Distribution function of $f_{\rm viaH}$ for $L = 512$.

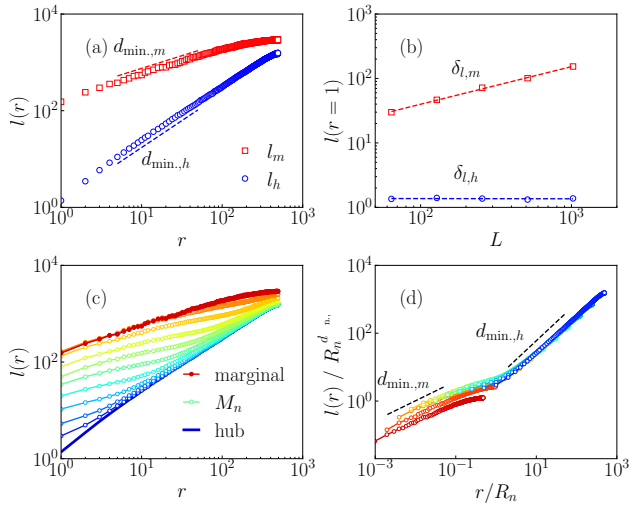

FIG. S5. (a) Chemical distance $l_{h/m}(r)$ from the hub/marginal site. (b) System size L dependence of $l_{h/m}(r = 1)$. These plots confirm the power law scaling of Eq. (7) with $\delta_h = 0$, $\delta_m \simeq 0.52$, $d_{\rm min.,h} \simeq 1.11$, and $d_{\rm min.,m} \simeq 0.58$. (c) Chemical distance $l_n(r)$ from the local minimum RWC site M_n. (d) Scaling plot of $l_n(r)/R_n^{d_{\rm min.,h}}$ against r/R_n. $L = 1024$ in (a), (c), and (d).

Appendix E: MFPT vs Chemical Distance

Structural heterogeneity of the critical percolation cluster is evidenced by the scaling behavior of the chemical distance $l(r)$ with respect to the Euclidean distance between two sites. The chemical distance between two sites is defined as the number of edges in the shortest path connecting them. It is known that the *average* chemical distance $l(r)$ between any pairs of sites at a distance r scales as $l(r) \sim r^{d_{\rm min.}}$ with the chemical distance exponent $d_{\rm min.}$ (Sec. 6.6 of [36]), which is for 2D critical percolation clusters $d_{\rm min.} \simeq 1.14$. We discriminate between

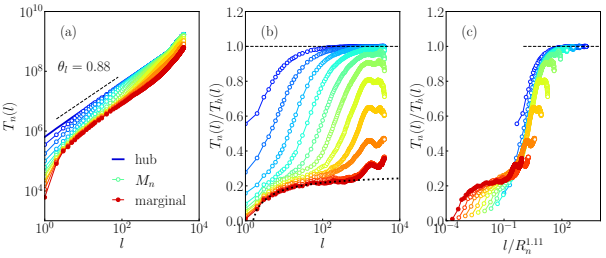

FIG. S6. (a) MFPT vs chemical distance from the hub and the local minimum RWC sites. (b) Ratio of $T_n(l)$ to $T_h(l)$ for $n \geq 1$. For the marginal site, $T_m(l)/T_h(l)$ can be fitted to a function $0.27 - 0.26/\ln(1.70l)$, which is drawn with a dotted line. (c) Scaling plot of $T_n(l)/T_h(l)$ against $l/R_n^{d_{\rm min.}}$.

the hub and the marginal site as starting site and find

$$l(r) \sim L^{\delta} r^{d_{\rm min.}} \tag{S1}$$

with *different* exponents $(\delta, d_{\rm min.}) = (\delta_h, d_{\rm min.,h}) \simeq (0.0, 1.11)$ for the hub and $(\delta_m, d_{\rm min.,m}) \simeq (0.52, 0.58)$ for the marginal site (see Figs. S5(a) and (b)), satisfying $\delta_h + d_{\rm min.,h} \simeq \delta_m + d_{\rm min.,m}$. The chemical distance $l_n(r)$ from the local minimum RWC site M_n shows again a crossover $l_n(r) = L^{\delta_h} R_n^{d_{\rm min.,h}} \mathcal{G}(l/R_n)$ for $1 \ll R_n \ll L$ (see Figs. S5(c) and (d)).

Given the similar crossover scaling of $T_n(r)$ and $l_n(r)$, one may anticipate a simple scaling, $T(l) \sim l^{\theta_l}$ with a unique exponent $\theta_l = \theta/d_{\rm min.}$, of the MFPT with respect to the chemical distance. Such a simple scaling behavior of the average MFPT was indeed reported in Ref. [17, 18]. We have investigated the source site dependence of the MFPT function $T_n(l)$. Figure S6(a) shows the $T_h(l)$ from the hub follows the power law scaling

$$T_h(l) \sim l^{\theta_l} \tag{S2}$$

with $\theta_l \simeq 0.88$. This exponent satisfies the scaling relation $\theta_l = \theta_h/d_{\rm min.,h}$. The MFPT $T_n(l)$ from the local minimum RWC sites still displays a crossover, albeit weak. The crossover is more evident in Fig. S6(b). $T_n(l)$ undergoes a crossover between two limiting behaviors, $T_h(l)$ of the hub and $T_m(l)$ of the marginal site, at a characteristic scale of the chemical distance $l_n \sim R_n^{d_{\rm min.}}$ (see Fig. S6(c)). The numerical data suggest that

$$T_m(l) = T_h(l)/(a - b/\ln(cl)) \tag{S3}$$

with $O(1)$ constants a, b, and c (see Fig. S6(b)). The logarithmic correction results in the slow convergence of the effective exponent in Fig. S2(d).

Appendix F: Number of bridge bonds

We investigate numerically the scaling law for the number of bridge bonds between the hub (highest RWC site)

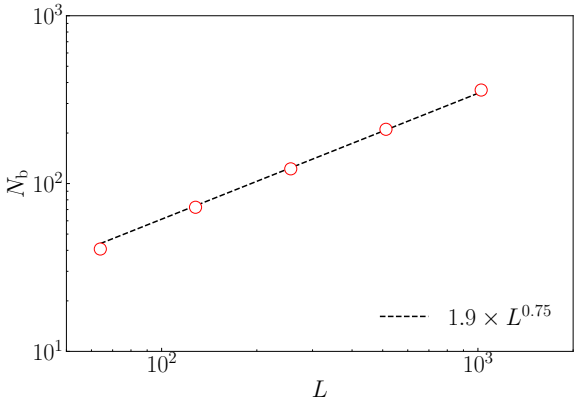

FIG. S7. The average number N_b of bridge bonds between the hub and the marginal site for on the 2D critical bond percolation clusters on the $L \times L$ square lattices.

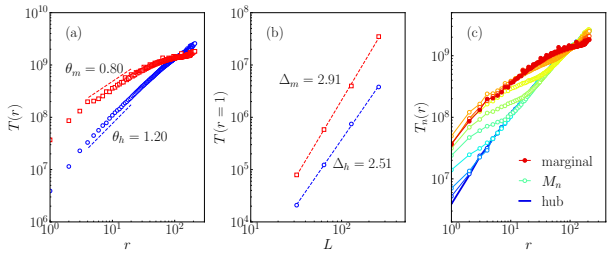

FIG. S8. MFPT on the critical bond percolation cluster in 3D. (a) MFPT $T(r)$ from the hub and the marginal site for $L = 256$. (b) Size dependence of the MFPTs from the hub and the marginal site to the sites at a distance $r = 1$. (c) MFPTs from the hub, the marginal site, and the local minimum RWC sites for $L = 256$.

and the marginal site (lowest RWC site) on the 2D critical bond percolation clusters. On a given realization of a critical percolation cluster on a $L \times L$ square lattice, we identify the hub and the marginal site, and count the number of bridge bonds between the pair. The number of bridge bonds N_b averaged over 1000 realizations are presented in Fig. S7. It follows a power law $N_b \sim L^{0.75}$ with respect to the system size L. We note that the scaling exponent coincides with the fractal dimension of the red bonds [37].

Appendix G: Crossover scaling for 3D critical percolation clusters, 3D random trails, and the Sierpiński gasket

The crossover scaling is not limited to the 2D critical percolation clusters. To confirm the generality of the crossover scaling, we performed additional numerical studies.

First, we investigated the scaling law for the MFPT

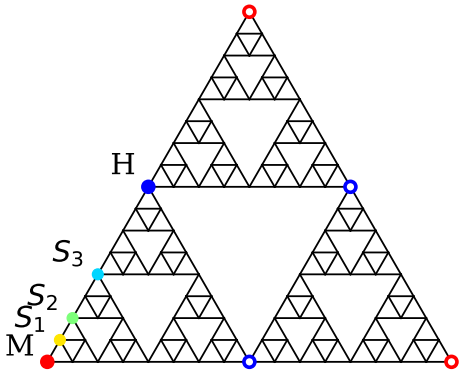

FIG. S9. Sierpiński gasket of the 5th generation. The three outermost sites are the marginal sites, and the three vertices of the largest empty triangle are the hubs. They are marked with red and blue symbols, respectively. The sites marked with filled symbols are the source sites for the study of MFPTs. An intermediate site S_n is at a distance 2^{n-1} from the marginal site.

$T(r)$ on the 3D critical bond percolation clusters. It is known that the critical threshold is given by $p_c \simeq 0.248\ 812\ 6$ and the fractal dimension is given by $d_f \simeq 2.523$ [41]. On a critical percolation cluster, we identified the hub (highest RWC site), M_n (local minimum RWC site within a sphere of radius $R_n = 2^{n-1}$ around the hub), and the marginal site (lowest RWC site). The MFPTs from these sites to the other sites were measured as a function of the distance r. The ensemble averaged MFPTs from the hub and the marginal site satisfy the scaling law $T(r) \sim L^{\Delta} r^{\theta}$ with $(\Delta_h, \theta_h) \simeq (2.51, 1.21)$ for the hub and $(\Delta_m, \theta_m) \simeq (2.91, 0.79)$ for the marginal sites (see Figs. S8(a) and (b)). The sums $\Delta_h + \theta_h$ and $\Delta_m + \theta_m$ are close to each other, and consistent with the random walk dimension $d_w \simeq 3.64 \pm 0.05$ [2]. Figure S8(c) demonstrates that the MFPTs $T_n(r)$ from the local minimum RWC sites display the crossover scaling behavior.

Second, we examined the MFPT on a random walk trail in 3D, which is itself a random fractal with $d_f = 2$ [42]. On an L^3 cubic lattice with periodic boundary conditions, we generated a random walk trail of $8L^2$ steps and explored the MFPT problem on top of it. Figure 4 (b) of the main text illustrates the distance dependence of outbound MFPTs from the hub, the local minimum RWC sites, and the marginal site. The MFPT scales as $T(r) \sim L^{2.00} r^{1.25}$ for the hub and $T(r) \sim L^{1.80} r^{1.52}$ for the marginal site, and exhibits a crossover scaling for the intermediate sites.

Lastly, we studied the scaling of the MFPT on the Sier-

piński gasket, a deterministic fractal. Figure S9 depicts a Sierpiński gasket of the 5th generation. As a deterministic fractal, it has a symmetric shape and a degenerate RWC distribution. To avoid ambiguity arising from this degeneracy, we considered the MFPTs from a hub, a marginal site, and intermediate sites $\{S_n\}$ on a straight line between them. Figure 4 (c) of the main text shows outbound MFPTs from the source sites on a Sierpiński gasket of the 10th generation.

The crossover scaling for the Sierpiński gasket is weak in comparison with the other fractals. The MFPT obeys the power-law scaling $T(r) \sim AL^{\Delta} r^{\theta}$ with *site-independent* universal scaling exponents $\Delta = d_f$ and $\theta = d_w - d_f$ with $d_f = \ln 3/\ln 2$ and $d_w = \ln 5/\ln 2$, where L is a linear size. Interestingly, the amplitude A displays a site-dependent crossover behavior between two values, A_H for the hub and A_M for the marginal site. The MFPT from S_n scales with the amplitude $\sim A_H$ in a short distance regime and with the amplitude $\sim A_M$ in a long distance regime. The Sierpiński gasket is a simple fractal characterized by a single fractal dimension d_f. It does not include any dangling ends, and there are not any bridge bonds between the hub and the marginal site. It might explain the reason why the scaling exponents are universal. Structural heterogeneity results in the weak crossover in the amplitude.